Journal of Sound and Vibration 329 (2010) 5356–5374

Contents lists available at ScienceDirect

Journal of Sound and Vibration

journal homepage: www.elsevier.com/locate/jsvi

Generalized asymptotic expansions for coupled wavenumbers in fluid-filled cylindrical shells

M.V. Kunte [a], Abhijit Sarkar [b], Venkata R. Sonti [a,*]

[a] Vibro-Acoustics Lab, Facility for Research in Technical Acoustics, Department of Mechanical Engineering, Indian Institute of Science, Bangalore 560 012, India
[b] Department of Mechanical Engineering, Indian Institute of Technology Madras, Chennai 600 036, India

ARTICLE INFO

Article history:
Received 17 February 2010
Received in revised form
29 April 2010
Accepted 12 June 2010
Handling Editor: L.G. Tham

ABSTRACT

Analytical expressions are found for the coupled wavenumbers in an infinite fluid-filled cylindrical shell using the asymptotic methods. These expressions are valid for any general circumferential order (n). The shallow shell theory (which is more accurate at higher frequencies) is used to model the cylinder. Initially, the *in vacuo* shell is dealt with and asymptotic expressions are derived for the shell wavenumbers in the high- and the low-frequency regimes. Next, the fluid-filled shell is considered. Defining a relevant fluid-loading parameter μ, we find solutions for the limiting cases of small and large μ. Wherever relevant, a frequency scaling parameter along with some ingenuity is used to arrive at an elegant asymptotic expression. In all cases, Poisson's ratio ν is used as an expansion variable. The asymptotic results are compared with numerical solutions of the dispersion equation and the dispersion relation obtained by using the more general Donnell–Mushtari shell theory (*in vacuo* and fluid-filled). A good match is obtained. Hence, the contribution of this work lies in the extension of the existing literature to include arbitrary circumferential orders (n).

1. Introduction

The study of dispersion curves in *in vacuo* and fluid-filled cylindrical shells has been carried out by many researchers in the past. Some of the most widely cited works are by Fuller [1], Fuller and Fahy [2] and by Pavic [3]. More recent works include those by Muggleton et al. [4] who have studied wave propagation in *in vacuo* shells experimentally and Maess et al. [5] who use a finite-element formulation to find dispersion curves in a fluid-filled circular cylindrical shell. Xu and Zhang [6] also present the dispersion curves for fluid-filled cylindrical shells via a numerical approach.

A detailed study using asymptotic methods on the effect of fluid-loading on elastic structures such as plates has been carried out by Crighton [7–10]. In recent literature, a few asymptotic studies on nonlinear structural acoustic systems have been presented by Sorokin [11–14] where techniques such as the method of multiple scales and matched asymptotic expansions were used to study the effect of fluid-loading on nonlinear elastic structures. Studies on structural acoustic waveguides have been recently presented by Sarkar and Sonti using the asymptotic methods [15–17].

In Sarkar and Sonti's work, the coupled dispersion equation was expressed as the *in vacuo* structural dispersion equation with a correction term due to the fluid. Then a perturbed solution to the structural wavenumber was found around the *in vacuo* solution, from which physical inferences could then be drawn with ease. A similar approach was used for the acoustical wavenumber also with a correction term due to the flexible structure. The analytical expression directly gave the shift in the uncoupled wavenumber due to coupling. Thus, one could understand the wavenumber shift as being

* Corresponding author.
E-mail address: sonti@mecheng.iisc.ernet.in (V.R. Sonti).

0022-460X/$ - see front matter © 2010 Elsevier Ltd. All rights reserved.
doi:10.1016/j.jsv.2010.06.028

due to a stiffness-like or an inertia-like effect of the structure/fluid on the fluid/structure, respectively. The Donnell–Mushtari (DM) theory was used to model the shell dynamics. Due to the complexity of the DM equations, it was easier to find solutions for a specific value of the circumferential order n and hence, the axisymmetric mode ($n=0$) and the beam mode ($n=1$) were dealt with separately. The axisymmetric mode is the simplest mode due to the decoupling of the torsional vibrations from the vibrations in the other two directions. The $n=1$ mode is the lowest-order mode for which the vibrations in all the three directions are coupled.

In this article, using matched asymptotic expansions (MAE) [18] we present general analytical expressions for the wavenumbers of any circumferential order in circular cylindrical shells (*in vacuo* and fluid-filled) based on the shallow shell theory (SST). The SST is known to be more accurate in the higher frequency range considering the assumptions made in its derivation [19]. Results exactly comparable with Heckl [20] and Fahy [21] for cylindrical shell dispersion relations have been presented by Sarkar and Sonti [22] using the SST. According to published literature, the accuracy of the SST is acceptable for the circumferential order $n \geq 2$. In this paper also we confine n to this range, i.e., $n \geq 2$. In the initial part of the paper, we deal with the *in vacuo* cylindrical shell where the wavenumber expressions for a general circumferential order are presented using high-frequency and low-frequency asymptotics. The asymptotic expansions involve the scaling parameter and Poisson's ratio. Then a fluid-filled infinite cylindrical shell is studied and the expressions for the coupled dispersion curves are presented. We confine our interest to the real wavenumbers. The increased simplicity in the form of the SST equations allows one to find analytical expressions for a general value of n. This is the principal contribution of this paper. Thus, the circumferential mode number n now appears as a parameter in our expansions along with μ (the fluid loading parameter) and ν (Poisson's ratio). For the *in vacuo* case, the accuracy of the expansions is checked against the direct numerical solutions of the dispersion equation from the SST and also against the numerical results from the DM theory, which is one of the commonly accepted thin shell theories [1–3]. For the fluid-filled cases, the asymptotic expansions are validated for their accuracy by comparing with the numerical results of the coupled dispersion equation and the calculations based on the fluid-filled shell equations derived using the DM shell theory. Finally, the universal constant-frequency loci for the coupled case are superposed on top of the *in vacuo* loci to gain additional insights.

We do mention here that we have used a regular perturbation method in every case studied in the paper. The matching of the solutions in the intermediate frequency zones is left out to keep the article length within limits. And there is no further insight to be gained by their inclusion. So, for the present work, MAE reduces to a set of regular perturbation solutions obtained in different frequency bands. We do call our method as MAE since it strictly falls in the context of MAE, and because the separate expansions can be matched.

We begin by deriving expressions for the uncoupled acoustic and structural wavenumbers.

2. Uncoupled analysis

2.1. Uncoupled acoustic wavenumbers

The solution to the wave equation for a wave travelling in the positive x-direction in a circular cylindrical duct (see Fig. 1) is as shown [23]

$$p(r,\theta,x,t) = PJ_n(k_s r)\cos(n\theta)e^{i(\omega t - k_x x)}, \tag{1}$$

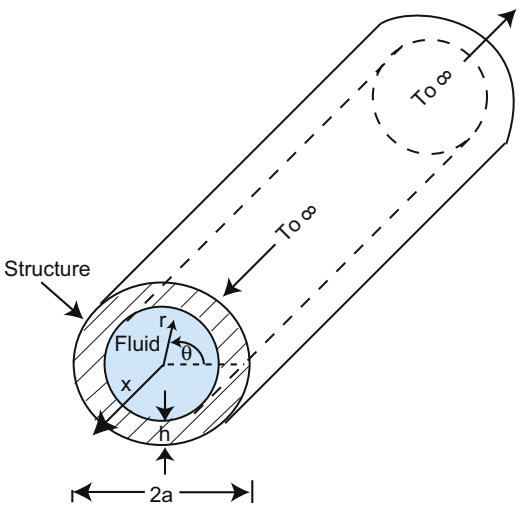

Fig. 1. Schematic of the infinite fluid-filled flexible cylindrical shell.

where P is the amplitude and $J_n(\ )$ is the n th-order Bessel function of the first kind. k_s and k_x are the radial and the axial wavenumbers, respectively. Note, $k_s^2+k_x^2=k^2=(\omega/c_f)^2$ where k is the acoustic wavenumber and c_f is the speed of sound in the fluid.

Based on the boundary condition at the duct wall, $r = a$, the solutions for the wavenumbers are given by

$$J_n'(k_s a)=0 \quad \text{for a rigid} - \text{walled cylindrical duct and}$$

$$J_n(k_s a)=0 \quad \text{for a pressure} - \text{release cylindrical duct.} \tag{2}$$

Solving the above equations, one gets the uncoupled rigid-duct and pressure-release wavenumbers (k_x). In the presence of a flexible structural boundary, we expect the coupled wavenumbers to be perturbations on these solutions. The intersection of these wavenumbers with the *in vacuo* bending wavenumber of the same circumferential order gives the respective coincidence frequencies, denoted as *rigid-duct* (*RD*) *coincidences* and *pressure-release* (*PR*) *coincidences*.

2.2. Uncoupled structural wavenumber

2.2.1. The SST

The shallow-shell theory, also referred to as the Donnell–Mushtari–Vlasov theory in the literature, is a simplification of the more general thin shell theories [19]. We briefly list the basic steps involved in the derivation of the thin shell equations here to highlight the differences of the SST from the thin shell theories. The basic steps are as follows:

1. Derivation of the equilibrium equations in terms of the forces and moments.
2. Application of the Love–Kirchoff Hypothesis to simplify these relations.
3. Calculation of force and moment resultants in terms of the stress components as integrals.
4. Substitution of the stress–strain constitutive relations in the force–momentum resultants.
5. Substitution of the strain–displacement relations into the stress–strain relations.
6. Integration of the force-stress and moment-stress relations after substituting the relations from the steps 4 and 5.
7. The assumptions made in selectively neglecting certain terms and keeping the others while performing the integrations are the main reason for the differing accuracies of different thin shell theories.

The SST differs from the thin shell theories in the following way:

1. Once the strains have been separated out into the membrane and bending components, the contributions of in-plane deflections are neglected in the bending strain expressions but not in the membrane strain expressions.
2. Secondly, the influence of inertia in the in-plane direction is neglected.
3. Finally, following the Love–Kirchoff Hypothesis in the thin shell case, the shear deflection and hence, shear strains, which are produced due to the shear stresses are assumed to be negligible and are dropped from subsequent analysis. However, the shear stresses themselves are significant and are used to calculate the force resultants. Here, even the shear stresses are assumed to be negligible, putting the shear force terms to zero.
4. The solution is carried out using an Airy-stress-function approach by which the equations of motion in the axial and circumferential directions are automatically satisfied by the choice of an appropriate stress function. Thus, from the equation of motion in the radial direction and the compatibility condition [24], we now have two equations in the two unknowns, radial displacement and the stress function as shown in the following section. In the case of the thin shell equations, we have three equations in the three displacement components.

As a result, the theory is limited to cases in which the above assumptions are valid, such as in shells with only a normal loading applied. Traditionally, this model was found to work well for shells with small curvatures though this is an '*unnecessarily strict restriction*' [19].

2.2.2. The in vacuo dispersion relation and numerical solution

The following derivation has already been presented in [22]. We reproduce the steps here for completeness before presenting the equation for the fluid-filled shell. The shallow shell differential equations for the free vibrations of circular cylindrical shells are given by (see [19, Sections 6.7–6.9])

$$D\nabla^4 w+\nabla_R^2\phi=q_n,$$

$$\nabla^4\phi-Eh\nabla_R^2 w=0. \tag{3}$$

Eliminating ϕ we get

$$D\nabla^8 w(\theta,x)+Eh\nabla_R^4 w(\theta,x)=\rho_s h\omega^2\nabla^4 w(\theta,x). \tag{4}$$

In the above equation, w is the radial displacement of the cylindrical shell, h is the shell thickness, ω is the circular frequency, ρ_s, E and ν are the density, Young's modulus of elasticity and Poisson's ratio of the shell material, respectively. The parameter D is the flexural rigidity given by $D=Eh^3/[12(1-\nu^2)]$.

Note, ∇^2, the Laplacian operator, and ∇_R^4 for a circular cylindrical shell are given by

$$\nabla^2 w=\frac{1}{a^2}\frac{\partial^2 w}{\partial\theta^2}+\frac{\partial^2 w}{\partial x^2},\quad \nabla_R^4 w=\frac{1}{a^2}\frac{\partial^4 w}{\partial x^4}\quad \text{(see [19, Eq. (6.9.2)])},$$

where a is the radius of the circular cylindrical shell.

Substituting the above operators in Eq. (4) and assuming a solution for w of the form $w(\theta,x)=W\cos(n\theta)e^{-ik_x x}$ where k_x is the bending wavenumber associated with the wave propagating in the axial direction, we get

$$\frac{1}{(1-\nu^2)}[(n\sqrt{\beta})^2+(\kappa\sqrt{\beta})^2]^2+\frac{(\kappa\sqrt{\beta})^4}{[(n\sqrt{\beta})^2+(\kappa\sqrt{\beta})^2]^2}=\Omega^2. \tag{5}$$

Here, κ is the non-dimensional wavenumber given by $\kappa=k_x a$ and β is the non-dimensional thickness parameter given by $\beta=h/(a\sqrt{12})$. Ω is the non-dimensional frequency given by $\Omega=\omega a/c_L$ where $c_L=\sqrt{E/\rho_s}$ is the extensional wave speed. But for the $(1-\nu^2)$ term, Eq. (5) is identical to Eq. (2.114) or Eq. (4.167) in [21] (original derivation in [20]). The effect of this term can be quantified for practical values of ν using the asymptotic expressions for the wavenumbers as will be shown later. Further, this relation holds for all n. This relation will be used in the analysis of the uncoupled structural wavenumbers.

In the following sections, we use the technique of matched asymptotic expansions (MAE) [18] to present asymptotic solutions to the above equation and compare them with the numerical solutions of the same. In the general application of this technique, a different scaling of terms is used in different regimes of the independent variable (Ω in our case) and using this, different solutions are obtained in each of these regions. The solutions are then patched together by an appropriate expansion for intermediate values of the independent variable. In this paper, we obtain separate expansions for the high- and low-frequency regimes and verify their accuracy against the commonly used DM theory. However, we do not find separate expansions in the intermediate frequency range.

2.2.3. Asymptotic solution—high frequency

Here, the first step is to rescale the variables so that the region of interest shifts towards the high frequency. This is done by employing the following transformation [16]:

$$\Omega=\frac{\Omega_{rs}}{\varepsilon},$$

$$\kappa=\frac{\kappa_{rs}}{\sqrt{\varepsilon}}, \tag{6}$$

where Ω_{rs} and κ_{rs} are the rescaled variables, both of $\mathcal{O}(1)$ magnitude. ε is a fictitious parameter of a small magnitude and is used to rescale the variables. ε is also used as an expansion parameter in the MAE solution. Additionally, it serves as an initial check with regard to the correctness of the asymptotic expansion obtained as ε must disappear in the final expression since it is an artificially introduced parameter. The rescaling used above in Eq. (6) is arrived at from understanding the physics since, at higher frequencies, the *in vacuo* shell behaves like a plate when the radius of curvature is much larger than the wavelength. Thus, we take the flexural wavenumber $\kappa\propto\sqrt{\Omega}$ which suggests the above transformation. However, to do it rigorously, the correct rescaling transformation should be obtained by choosing the powers of ε as variables in the asymptotic expansion, substituting this expansion in the equation and balancing the powers of ε in the dominant terms after rescaling [18].

We substitute the transformation given in Eq. (6) into the dispersion relation (Eq. (5)). To find the solution for κ_{rs}, we use $\kappa_{rs}=\kappa_0+\varepsilon a_1+\nu^2 b_1$ in the rescaled dispersion relation and perform a double series expansion about $\varepsilon=0$ and $\nu=0$. The choice of the ν^2 term in the expansion is made after having tried expansions with a linear term in ν term and having found its coefficient to be zero. These are standard steps in the procedure to solve problems using asymptotic methods [18]. Solving at each order of ε and ν^2 and retaining only the first-order corrections, we get the following asymptotic expression:

$$\kappa_{rs}=\sqrt{\frac{\Omega_{rs}}{\beta}}-\varepsilon\frac{1}{2}n^2\sqrt{\frac{\beta}{\Omega_{rs}}}-\frac{1}{4}\nu^2\sqrt{\frac{\Omega_{rs}}{\beta}}. \tag{7}$$

This in the original variables κ and Ω is given by

$$\kappa=\sqrt{\frac{\Omega}{\beta}}-\frac{1}{2}n^2\sqrt{\frac{\beta}{\Omega}}-\frac{1}{4}\nu^2\sqrt{\frac{\Omega}{\beta}}. \tag{8}$$

2.2.4. Asymptotic solution—low frequency

In the low frequency region, we again follow a similar approach as before, i.e., rescale the equation with an artificial parameter (ε). Thus, the transformation employed is as follows:

$$\beta = \varepsilon b,$$

$$\Omega = \Omega_{rs}\varepsilon,$$

$$\kappa = \kappa_{rs}\sqrt{\varepsilon}. \tag{9}$$

The additional transformation equation for β is necessary as in the low-frequency range, the assumption that the shell is thin is especially important and needs to be invoked explicitly by setting β to be of $\mathcal{O}(\varepsilon)$. The other two relations are obtained as earlier by using an order-balancing argument.

The perturbed wavenumber is obtained as follows:

$$\kappa_{rs} = \sqrt[4]{-n^4b^2+\Omega_{rs}^2}\,n - \varepsilon\frac{1}{2}\frac{n(-\Omega_{rs}^2+2n^4b^2)}{\sqrt[4]{-n^4b^2+\Omega_{rs}^2}} - \nu^2\frac{1}{4}\frac{b^2n^5}{(-n^4b^2+\Omega_{rs}^2)^{3/4}}. \tag{10}$$

Rescaling back to the original variables, the final equation is

$$\kappa = \sqrt[4]{-n^4\beta^2+\Omega^2}\,n - \frac{1}{2}\frac{n(-\Omega^2+2n^4\beta^2)}{\sqrt[4]{-n^4\beta^2+\Omega^2}} - \nu^2\frac{1}{4}\frac{\beta^2n^5}{(-n^4\beta^2+\Omega^2)^{3/4}}. \tag{11}$$

The comparison of the asymptotic and the numerical solutions of Eq. (5) is shown in Fig. 2. Also shown in the figure are the dispersion curves obtained from the numerical solution of the DM theory [25]. These dispersion curves have been presented for a shell with h/a=0.05, i.e., $\beta = h/(a\sqrt{12}) = 0.0144$.

2.3. Validity of the asymptotic series

In this section, we study the validity of the above expansions following the standard procedure in Hinch [18] and Nayfeh [26].

2.3.1. High-frequency expansion

Restating Eq. (8) here for clarity, the asymptotic expansion for the high-frequency *in vacuo* structural wavenumber is given by

$$\kappa = \sqrt{\frac{\Omega}{\beta}} - \frac{1}{2}\frac{n^2}{\sqrt{\frac{\Omega}{\beta}}} - \nu^2\frac{1}{4}\sqrt{\frac{\Omega}{\beta}}. \tag{12}$$

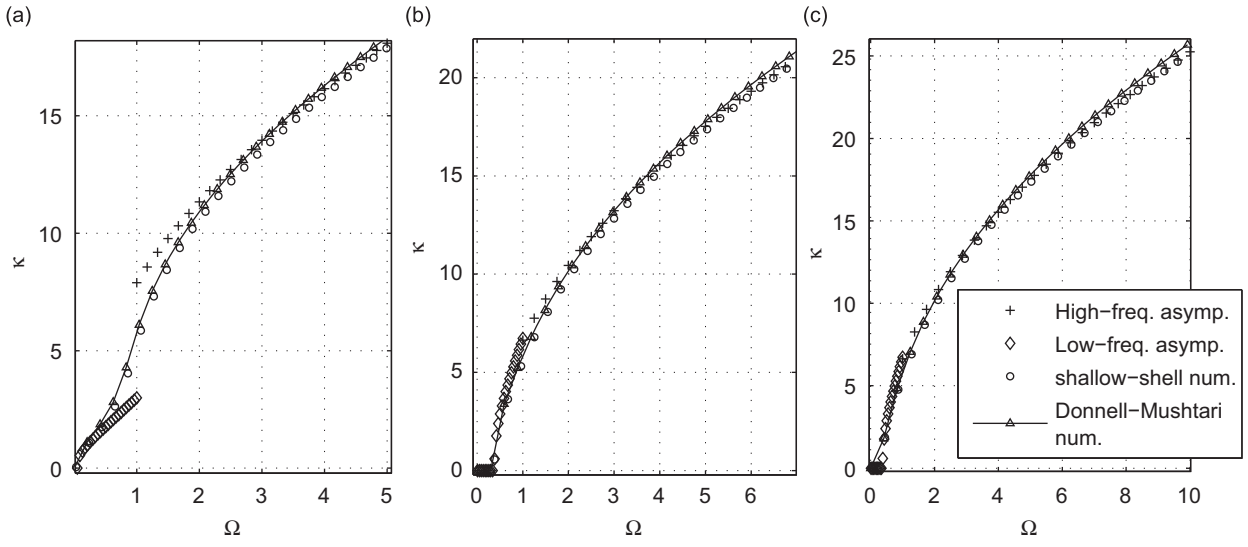

Fig. 2. Dispersion curves for *in vacuo* shell—comparison of high- and low-frequency asymptotic solutions (Eqs. (8) and (11)) with the numerical solution for the SST and the DM theory—$\beta = 0.0144$, $\nu = 0.3$, (a) n=2, (b) n=5, (c) n=10.

To study the validity of the above series, it is re-written as follows:

$$\kappa = \sqrt{\frac{\Omega}{\beta}}\left[1-\frac{1}{2}\frac{n^2}{\left(\frac{\Omega}{\beta}\right)}-v^2\frac{1}{4}\right]. \tag{13}$$

Looking at the terms in the square-brackets it can be seen that the coefficient of v^2, viz., 0.25, is constant and is much lesser than $\mathcal{O}(1/v^2)$. Being a constant it stays bounded for all values of n and Ω and never causes the expansion to become invalid. For the correction term corresponding to ε, we have

$$\frac{n^2}{\left(\frac{\Omega}{\beta}\right)} \ll \mathcal{O}(1).$$

Thus, for a given n, as one goes higher in frequency and the shell becomes thinner, the expansion becomes more accurate.

2.3.2. Low-frequency expansion

Again, restating Eq. (11) here for clarity, the asymptotic expansion for the low-frequency *in vacuo* structural wavenumber is given by

$$\kappa = \sqrt[4]{-n^4\beta^2+\Omega^2}\,n-\frac{1}{2}\frac{n(-\Omega^2+2n^4\beta^2)}{\sqrt[4]{-n^4\beta^2+\Omega^2}}-v^2\frac{1}{4}\frac{\beta^2n^5}{(-n^4\beta^2+\Omega^2)^{3/4}}, \tag{14}$$

which is rewritten as follows:

$$\kappa = \sqrt[4]{-n^4\beta^2+\Omega^2}\,n\left[1-\frac{1}{2}\frac{(-\Omega^2+2n^4\beta^2)}{\sqrt{-n^4\beta^2+\Omega^2}}-v^2\frac{1}{4}\frac{\beta^2n^4}{(-n^4\beta^2+\Omega^2)}\right]. \tag{15}$$

Thus, observing the leading-order term, for the wavenumber to be real, $\Omega > n^2\beta$. From the next term, we have

$$\frac{(-\Omega^2+2n^4\beta^2)}{\sqrt{-n^4\beta^2+\Omega^2}} \ll \mathcal{O}(1).$$

Finally, from the coefficient of the v^2 term,

$$\frac{\beta^2n^4}{(-n^4\beta^2+\Omega^2)} \ll \mathcal{O}\left(\frac{1}{v^2}\right).$$

Thus, the region of validity of the low-frequency expansion is given by the intersection of the regions of validity given by the above inequalities.

2.4. Insights into results from in vacuo expansions

From the nature of expansions and Fig. 2, we draw some inferences.

1. In the high frequency expansion (Eq. (8)), the linear term in v is absent. The first non-zero correction is second order in v.
2. The coefficient of v^2 being constant, it never causes the expansion to become invalid.
3. In the high-frequency expansion, the correction term corresponding to ε is proportional to $n^2\Omega^{-1/2}$. For a very high frequency for a given n, the correction term being proportional to $\Omega^{-1/2}$ tends to zero, i.e., the behaviour approaches that of a true plate. For n values where the correction term $n^2\Omega^{-1/2}$ is small, we expect the curves for these n to stack up very close to each other, since the leading-order term is independent of n. This is also seen in the numerical solutions.
4. From the low frequency expansion, it is seen that the wavenumber κ becomes real when $\Omega > n^2\beta$. On the other hand, solving the governing equation (Eq. (5)) gives $\Omega = n^2\beta/(1-v^2)$ as the exact cut-on frequency. Using a binomial expansion it can be seen that the approximate value as predicted by the asymptotic expansion differs from the exact value by $\mathcal{O}(v^2)$ which is an acceptable degree of error.
5. Also from the second term in the rewritten low-frequency *in vacuo* structural wavenumber, it can be seen that for a given n, the term is proportional to Ω and hence its accuracy also decreases with Ω.
6. In general, as seen from Fig. 2, the expansions match well with the numerical solutions and with the DM theory. This validates the use of the SST and asymptotic methods.

The numerical solutions here have been obtained by using a numerical implementation of the established continuation technique. Here, an initial guess is made for one point on the solution curve. A MATLAB root-finding routine is invoked to

find a solution point using this initial guess as an initial condition. We then march ahead in frequency and the previous solution point is used as an initial condition for the next point on the solution curve and so on. In our implementation, since the high-frequency behaviour is known, we make an initial guess for the point corresponding to the highest frequency that we seek a solution for. On the basis of this, the initial value chosen is $\kappa_{\text{guess}} = \sqrt{\Omega_{\max}/\beta}$ where $\Omega_{\max}$ is the maximum value of Ω for which the solution is sought. We then march backward in frequency, in this case towards zero, to get the complete dispersion curve.

3. Fluid-filled shell

3.1. Coupled dispersion equation

In this section, the fluid-filled shallow-shell model is considered. We start with the structural equation with an additional loading term from the acoustic pressure, briefly described below.

As shown in Eq. (1), the solution to the wave-equation in cylindrical coordinates is

$$p(r,\theta,x,t) = PJ_n(k_s r)\cos(n\theta)e^{i(\omega t - k_x x)},$$

where $k_s^2 + k_x^2 = \omega^2/c_f^2$, $J_n(\ )$ is the nth-order Bessel function of the first kind.

Imposing the velocity continuity condition at $r=a$ using Euler's equation we get

$$\omega^2 \rho_f w = \left.\frac{\partial p}{\partial r}\right|_{r=a}. \tag{16}$$

Substituting $w(\theta,x,t) = W\cos(n\theta)e^{i(\omega t - k_x x)}$ (see Section 2) and simplifying, we get

$$P = \frac{\omega^2 \rho_f}{k_s J_n'(k_s a)} W,$$

where W is the amplitude of the radial displacement and ρ_f is the fluid density.

The basic shell equations according to the shallow shell theory have been presented in Eq. (3) [19,27]. For the coupled case, the internal acoustic fluid introduces an additional term acting on the shell surface in the form of the acoustic pressure. Therefore, substituting for q_n and eliminating ϕ, the equation is as follows:

$$D\nabla^8 w + Eh\nabla_R^4 w = \rho_s h\omega^2 \nabla^4 w + \nabla^4 p,$$

$$D\nabla^8 w + Eh\nabla_R^4 w = \rho_s h\omega^2 \nabla^4 w + \frac{\omega^4}{c_f^4} p,$$

where

$$\nabla^4 p = \nabla^2(\nabla^2 p) = -\frac{\omega^2}{c_f^2}\left(-\frac{\omega^2}{c_f^2} p\right) = \frac{\omega^4}{c_f^4} p \tag{17}$$

and all the symbols are as defined in Section 2. Substituting for p and w, cancelling the common terms and simplifying, we get

$$D\left(\frac{n^2}{a^2} + k_x^2\right)^4 + Eh\frac{k_x^4}{a^2} = \rho_s h\omega^2\left(\frac{n^2}{a^2} + k_x^2\right)^2 + \frac{\omega^4}{c_f^4}\frac{\omega^2 \rho_f}{k_s J_n'(k_s a)} J_n(k_s a). \tag{18}$$

Introducing the following non-dimensional parameters $\kappa = k_x a$, $\Omega = \omega a/c_L$, $c = c_L/c_f$, $\zeta = k_s a = \sqrt{\Omega^2 c^2 - \kappa^2}$ and $\mu = \rho_f a/\rho_s h$ which is the fluid-loading parameter, we get the coupled dispersion equation as follows [27]:

$$\frac{\beta^2}{1-\nu^2}(n^2+\kappa^2)^4 + \kappa^4 - \Omega^2(n^2+\kappa^2)^2 - \Omega^6 c^4 \mu\left[\frac{J_n(\zeta)}{\zeta J_n'(\zeta)}\right] = 0. \tag{19}$$

The last term involving μ is the coupling term and can be used to classify the kind of loading as mass-like or stiffness-like based on its sign. The fluid-loading parameter μ is a measure of the ratio of the mass per unit area of the fluid to the mass per unit area of the shell. In the following analysis, we find asymptotic solutions in the limit that $\mu = 0$ or $\mu = \infty$, i.e., μ and $1/\mu$ are used as the asymptotic expansion variables, respectively.

In the expansion for the coupled structural wavenumber, a rescaling parameter is used again along with Poisson's ratio. It will be shown through calculations that the coupled fluid wavenumbers (the RD and the PR) do not depend on Poisson's ratio (ν) at $\mathcal{O}(\nu^2)$. In all the cases, the expansion is compared with the numerical solution and the fluid-filled shell curves derived using the Donnell–Mushtari (DM) theory, denoted as DM(ff) theory, where 'ff' stands for 'fluid-filled'.

3.2. Limiting solutions

Eq. (19) is rewritten as

$$\underbrace{\left[\frac{\beta^2}{1-\nu^2}(n^2+\kappa^2)^4+\kappa^4-\Omega^2(n^2+\kappa^2)^2\right]}_{S}\underbrace{\zeta}_{PW}\underbrace{J_n'(\zeta)}_{R}-\Omega^6c^4\mu J_n(\zeta)=0. \tag{20}$$

We set $\mu=0$ and obtain the following limiting solutions; S=0 is the uncoupled structural solution and is identical to Eq. (5) obtained earlier, PW=0 is the plane-wave solution (not discussed) and R=0 is the uncoupled acoustic rigid-duct cut-on solution (first equation in Eq. (2)). Thus, for $\mu\ll1$, the asymptotic solutions for the coupled wavenumbers will be perturbations to these solutions. Alternatively, setting $\mu=1/\eta$ and rewriting the original equation, we have

$$\left[\frac{\beta^2}{1-\nu^2}(n^2+\kappa^2)^4+\kappa^4-\Omega^2(n^2+\kappa^2)^2\right]\zeta J_n'(\zeta)\eta-\Omega^6c^4\underbrace{J_n(\zeta)}_{PR}=0. \tag{21}$$

Setting $\eta=0$ which is the limiting case corresponding to $\mu=\infty$, we get PR=0 which is the uncoupled acoustic pressure-release cut-on solution (second equation in Eq. (2)).

Referring to the schematic (Fig. 3), S=0 gives the *in vacuo* structural wavenumber, R=0 is defined here as the 'uncoupled acoustic rigid-duct (RD) cut-on wavenumber' and referred to subsequently as such. Similarly, PR=0 is defined here as the 'uncoupled acoustic pressure-release (PR) cut-on wavenumber'.

3.3. Asymptotic results—coupled case

3.3.1. Case I: small μ

Here, we present the coupled wavenumbers for the small-μ case, i.e., where the fluid is much lighter than the structure. For convenience, Fig. 4 shows the schematic of the coupled wavenumbers that will be presented in this section. This figure will be referred to in the write-up below. One should note that the uncoupled structural wavenumber intersects with the uncoupled RD cut-ons and the uncoupled PR cut-ons. These intersections are denoted as the RD coincidences and the PR coincidences, respectively, as shown in Fig. 3.

As discussed earlier, the two solutions obtained for the small-μ case are the perturbations on the uncoupled RD cut-on wavenumber (R=0) and the perturbation on the *in vacuo* structural wavenumber (S=0), respectively. As will be shown from the derived asymptotic solutions, both these coupled solutions become invalid around the RD coincidence frequency. However, the coupled structural wavenumber is valid below the first RD coincidence and in intervals around each uncoupled PR coincidence. The coupled RD and coupled structural solutions can be patched together by an irregular perturbation expansion around an RD coincidence obtained by a different rescaling of the variables. We do not present this patching solution since this would make the document lengthy and it does not lead to any additional insights.

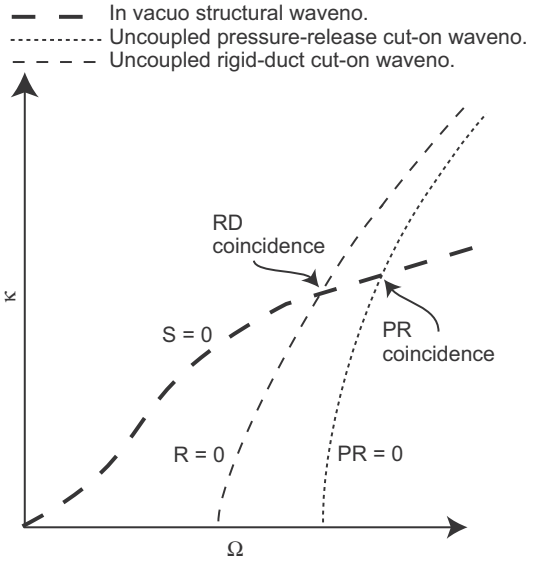

Fig. 3. Schematic of uncoupled wavenumbers.

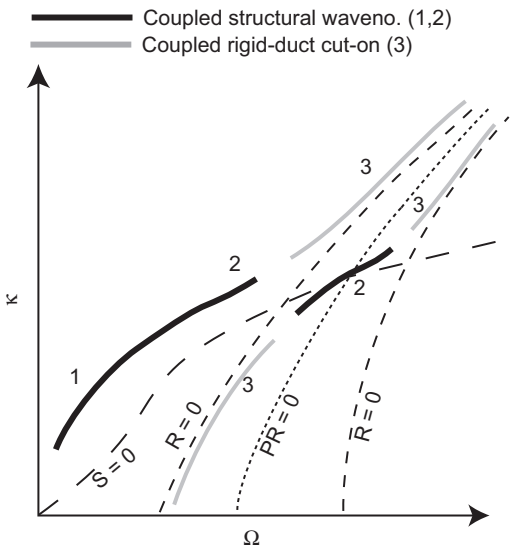

Fig. 4. Schematic of coupled wavenumbers, small μ case.

In the schematic figure (Fig. 4), Section 1 corresponds to the low-frequency coupled structural wavenumber. Section 2 represents the high-frequency coupled structural wavenumber. This solution is also valid in an interval around each PR coincidence. Section 3 represents the coupled RD cut-on wavenumber.

Also, the plane-wave perturbation solution corresponding to the limiting solution $PW=0$ has not been discussed here as this is a trivial solution (the amplitude of the pressure wave is uniformly zero inside the cylindrical cavity) for $n \geq 2$.

Coupled rigid-duct cut-on wavenumber: We start with the coupled dispersion relation as shown in Eq. (20). A regular perturbation approach is chosen without a frequency scaling. We choose an asymptotic expansion for κ of the form $\kappa = \kappa_0 + \mu a_1 + \nu^2 b_1$ and substitute this in the coupled dispersion relation. Simplifying this equation and balancing at orders yields the solution presented below:

$$\kappa = \kappa_0 + \mu \frac{\Omega^6 c^4 \zeta_0^2}{\kappa_0 (n^2 - \zeta_0^2) \underbrace{[\beta^2 (\kappa_0^2 + n^2)^4 + \kappa_0^4 - \Omega^2 (\kappa_0^2 + n^2)^2]}_{S'}}, \tag{22}$$

where $\zeta_0 = \sqrt{c^2\Omega^2 - \kappa_0^2}$ and κ_0 is given by the solution of $J_n'(\sqrt{c^2\Omega^2 - \kappa_0^2}) = 0$. As expected, the leading-order term in this solution is that given by $R=0$ in the coupled dispersion relation. From the asymptotic expression (Eq. (22)), it can be seen that the correction term corresponding to ν^2 goes to zero. This can be explained by the fact that ν is a structural parameter. Thus, the effect of the coupling of motions of the shell in different directions due to Poisson's effect on the dominantly acoustic coupled RD cut-on wavenumber can be expected to be seen only at a higher order.

The denominator of the correction term corresponding to μ contains the factor κ_0. Thus, when $\kappa_0 = 0$, i.e., at the uncoupled RD cut-on frequency, this asymptotic expression breaks down. Another factor of the denominator is S' which is equal to S as defined in the coupled dispersion relation (Eq. (5)) after setting $\nu = 0$. When $S' = 0$, we get the uncoupled RD coincidence frequency which is correct to $\mathcal{O}(\nu^2)$. Thus, Eq. (22) breaks down as we approach the uncoupled RD coincidence frequency. Alternative valid expansions can be found for both the above frequency regimes. Note that the coupled cut-on frequency is higher than the corresponding uncoupled one.

Fig. 5 presents the asymptotic solution obtained above plotted against the numerical solutions of the coupled dispersion equation (Eq. (20)) for various n. The match between the curves is seen to be good. As an added check, these solutions have been compared with the numerical solution of the dispersion equation for a fluid-filled shell as obtained by using the DM(ff) theory [1–3,25]. This solution again matches well with the solutions of the shallow-shell equation, validating the use of this shell theory. The results presented in this section are for a shell with $h/a=0.05$, i.e., $\beta = 0.0144$.

Coupled structural wavenumber: The coupled structural solution is expected to be a perturbation on the *in vacuo* structural solution given by $S=0$ in Eq. (20). For simplicity of the final solution and convenience of interpretation, we find an asymptotic solution which uses three asymptotic expansion parameters, namely μ, the fluid-loading parameter defined earlier, a frequency-scaling parameter, ε, which is actually a fictitious parameter and does not appear in the final solution, and ν Poisson's ratio.

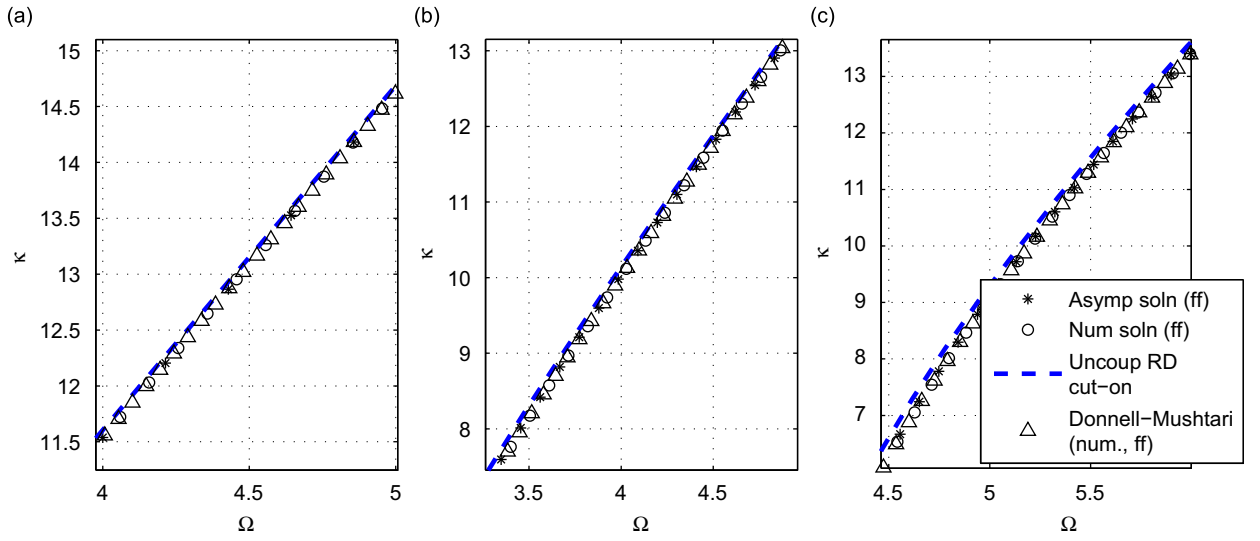

Fig. 5. Coupled rigid-duct cut-ons (Eq. (22)—(asymp, ff))—$\beta=0.0144$, $\nu=0.3$, $\mu=0.3$, $c=3$; (a) $n=2$, (b) $n=5$, (c) $n=10$ (Section 3 in Fig. 4). 'ff' stands for 'fluid-filled'.

Following Section 2.2 (as in Eq. (6)), we start with a high-frequency transformation to rescale κ and Ω. We then let $\kappa_{rs}=\kappa_0+\mu a_1+\varepsilon b_1+\nu^2 c_1$, where ε as said above is the frequency-scaling parameter. However, the form of the dispersion equation so obtained is complicated and poses some problems while working with the symbolic Math package MAPLE which was used in getting all the results. For this reason, we use a novel method to circumvent this problem.

Here, we start with a regular perturbation approach in one asymptotic expansion variable μ, i.e., $\kappa=\kappa_0+\mu\kappa_1$. Substituting in Eq. (20), at $\mathcal{O}(1)$, we have

$$\begin{aligned}&\beta^2\kappa_0^8+4\beta^2n^2\kappa_0^6+(-\Omega^2+6\beta^2n^4-\nu^2+\nu^2\Omega^2+1)\kappa_0^4\\&+\cdots(4\beta^2n^6+2\nu^2\Omega^2n^2-2\Omega^2n^2)\kappa_0^2+\beta^2n^8+\nu^2\Omega^2n^4-\Omega^2n^4=0.\end{aligned}\tag{23}$$

This equation cannot be easily solved to give closed-form expressions for κ_0. To solve this equation we now apply the high-frequency transformation (Eq. (6)) for the variables Ω and κ_0. The assumption implicit in this step is that κ_0 is the dominant term in the expression for κ which is a property of asymptotic series in general. Thus, instead of applying the frequency-scaling to the original variable κ, we apply the transformation to the leading-order term in the expansion. As we show later, the validity of this assumption is proven by our results. Using this method we solve the modified equation at $\mathcal{O}(1)$ by expanding κ_0 using two asymptotic expansion variables, ε and ν^2, and the solution for κ_0 is obtained as

$$\begin{aligned}\kappa_0\ (\text{rescaled})\ &=\sqrt{\frac{\Omega_{rs}}{\beta}}-\varepsilon\frac{1}{2}n^2\sqrt{\frac{\beta}{\Omega_{rs}}}-\frac{1}{4}\nu^2\sqrt{\frac{\Omega_{rs}}{\beta}},\\\kappa_0\ (\text{original variables})\ &=\sqrt{\frac{\Omega}{\beta}}-\frac{1}{2}n^2\sqrt{\frac{\beta}{\Omega}}-\frac{1}{4}\nu^2\sqrt{\frac{\Omega}{\beta}}.\end{aligned}\tag{24}$$

This is the same as Eq. (8) (high-frequency *in vacuo* structural wavenumber) and hence this method is validated. This solution is now substituted in the $\mathcal{O}(\mu)$ equation which gives the correction terms corresponding to μ as a function of κ_0. The final solution is as follows:

$$\kappa=\kappa_0-\frac{1}{4}\mu\left[\frac{\Omega^6c^4J_n(\zeta_0)(-1+\nu^2)}{\kappa_0\zeta_0J_n'(\zeta_0)\{2\beta^2\kappa_0^6+6\beta^2n^2\kappa_0^4+(-\Omega^2+6\beta^2n^4-\nu^2+\nu^2\Omega^2+1)\kappa_0^2+\nu^2\Omega^2n^2+2\beta^2n^6-\Omega^2n^2\}}\right],\tag{25}$$

where $\zeta_0=\sqrt{c^2\Omega^2-\kappa_0^2}$ as in Eq. (22).

It can be readily observed from the above expression that the factor $J_n'(\zeta_0)$ appears in the denominator of the correction term. This is the term R as defined in the coupled dispersion relation (Eq. (20)). Thus, as the frequency approaches the uncoupled RD coincidence frequency, $R=0$ and this asymptotic expansion breaks down. Also, the numerator of the correction term contains the factor $J_n(\zeta_0)$. This is the term PR as defined earlier (Eq. (21)). This term is zero at the PR coincidence frequency and the uncoupled and coupled structural wavenumbers coincide at this frequency.

Looking at the form of the equation after substituting for κ_0, we see that the expression obtained is equivalent to a three-variable expansion in μ, ν^2 and ε. The coefficient of μ contains ε and ν^2 implicitly through the solution for κ_0 and can

be said to contain the higher-order terms in ε and v^2 as well. A similar approach is also followed for the low-frequency region using the transformation given in Eq. (9). The correction term remains the same as in Eq. (25). The solution for κ_0 however is now obtained as follows:

$$\kappa_0 = \sqrt[4]{-n^4\beta^2+\Omega^2}\,n - \frac{1}{2}\frac{n(-\Omega^2+2n^4\beta^2)}{\sqrt[4]{-n^4\beta^2+\Omega^2}} - v^2\frac{1}{4}\frac{\beta^2 n^5}{(-n^4\beta^2+\Omega^2)^{3/4}}. \tag{26}$$

Again, this low-frequency solution for κ_0 is the same as that obtained in Eq. (11). We have compared these results against a full numerical solution of Eq. (20) and the DM(ff) theory as given by [1] to test the applicability of this method, as the use of such an approach has not come to our notice in the literature. The plots for the low-frequency region are as shown in Fig. 6 and the high frequency plots for a frequency just below the first coincidence are shown in Fig. 7.

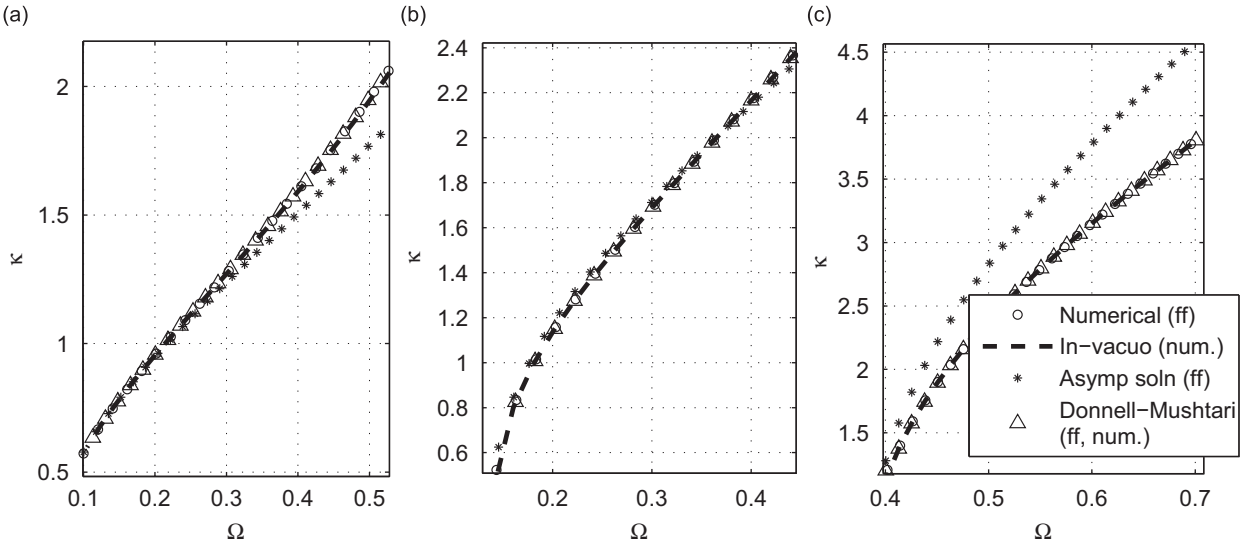

Fig. 6. Low-frequency coupled structural wavenumber—asymptotic (Asymp, ff) and numerical curves (num, ff) along with *in vacuo* structural numerical solution (*In vacuo*, num)—(Eqs. (26) and (25), far below 1st coincidence)—$\beta = 0.0144$, $v = 0.3$, $\mu = 0.3$, c=3; (a) n=2, (b) n=3, (c) n=5 (Section 1 in Fig. 4). 'ff' stands for 'fluid-filled'.

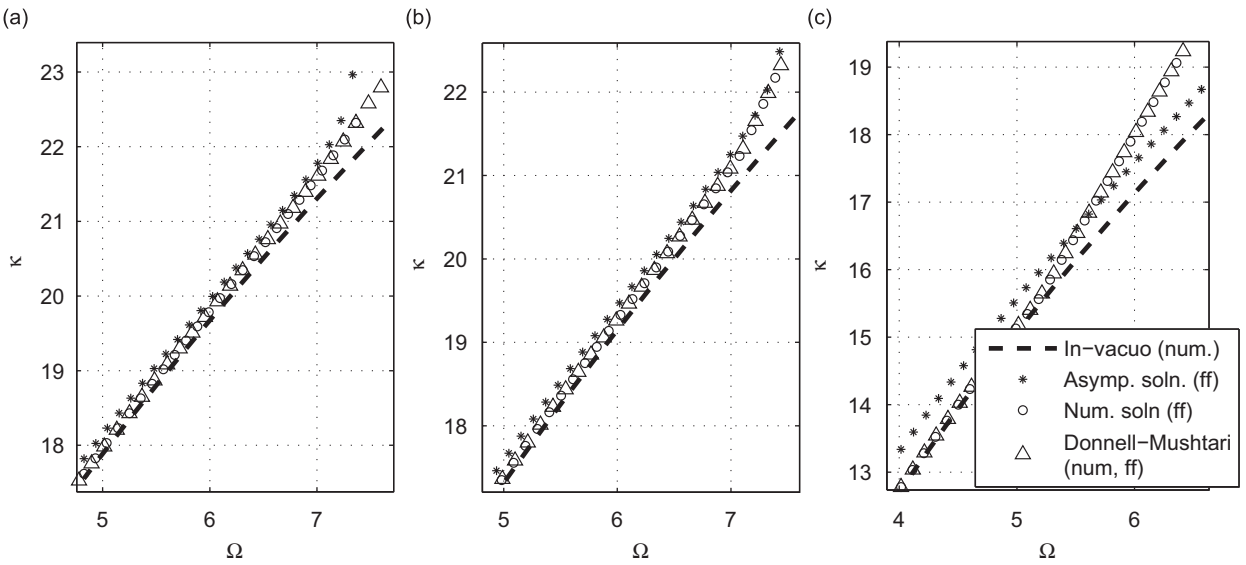

Fig. 7. High-frequency coupled structural wavenumber—asymptotic (Asymp, ff) and numerical curves (num, ff) along with *in vacuo* structural numerical solution—(*In vacuo*, num)—(Eqs. (24) and (25), at a frequency near but less than the 1st coincidence)—$\beta = 0.0144$, $v = 0.3$, $\mu = 0.3$, c=3; (a) n=2, (b) n=5, (c) n=10 (Section 2 in Fig. 4 below coincidence). 'ff' stands for 'fluid-filled'.

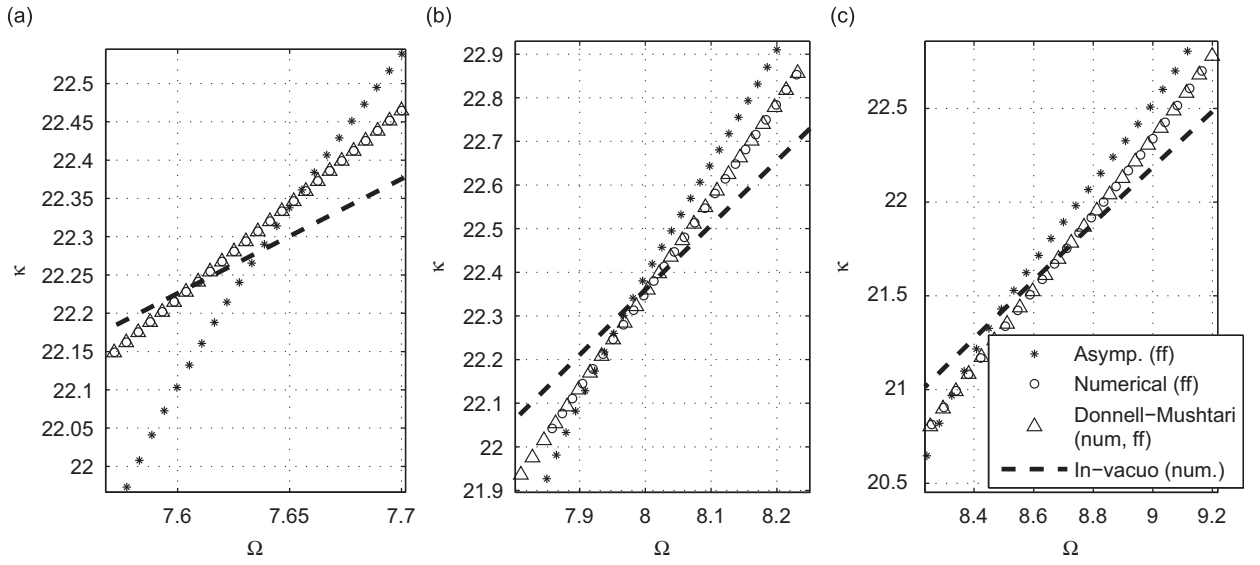

Fig. 8. High-frequency coupled structural wavenumber at 1st coincidence—asymptotic (Asymp, ff) and numerical curves (num, ff) along with *in vacuo* structural numerical solution—(*In vacuo*, num)—(Eqs. (24) and (25))—$\beta = 0.0144$, $\nu = 0.3$, $\mu = 0.3$, c=3; (a) n=2, (b) n=5, (c) n=10 (Section 2 in Fig. 4 at 1st coincidence). 'ff' stands for 'fluid-filled'.

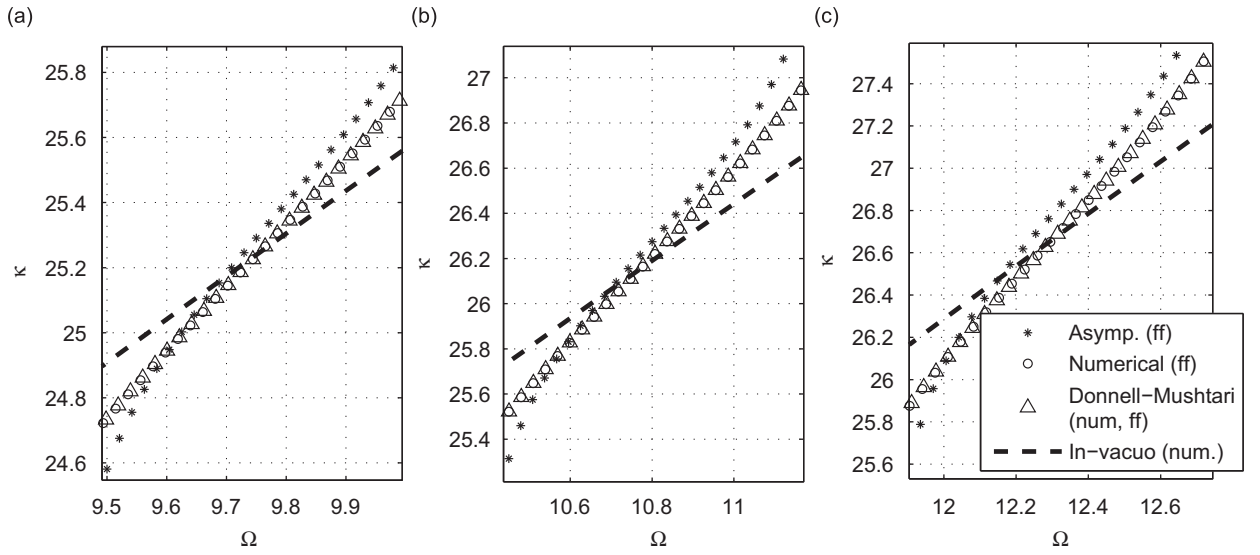

Fig. 9. High-frequency coupled structural wavenumber at 4th coincidence—asymptotic (Asymp, ff) and numerical curves (num, ff) along with *in vacuo* structural numerical solution—(*In vacuo*, num)—(Eqs. (24) and (25)), $\beta = 0.0144$, $\nu = 0.3$, $\mu = 0.3$, c=3; (a) n=2, (b) n=5, (c) n=10 (Section 2 in Fig. 4 at higher frequencies). 'ff' stands for 'fluid-filled'.

Since in the uncoupled RD coincidence region the coupled RD cut-on wavenumber blows up as discussed earlier, the appropriate solution is the coupled structural solution (Section 2 in the low-μ schematic (Fig. 4)). This solution is compared with the numerical solution and the DM(ff) theory in Fig. 8. The coupled structural solution patches the coupled rigid duct solutions on either side of the coincidence. This implies that in this region the nature of the wave transitions from being dominantly acoustic to being dominantly flexural and back to dominantly acoustic. This solution at the uncoupled PR coincidence region (the coupled structural wavenumber) gets more accurate for higher frequencies as shown in Fig. 9. The match between the asymptotic expansion and the numerical solution may appear to be questionable but this is a visual effect. This is due to consecutive uncoupled PR coincidence frequencies for a given n being densely clustered, resulting in the asymptotic solution breaking down for a frequency which is not very far from the uncoupled PR coincidence frequency.

3.3.2. Case II: large μ

In this case, as shown from Eq. (21), after replacing μ by $1/\eta$, with $\eta \ll 1$ being the asymptotic expansion parameter, there is only one limiting solution corresponding to PR=0, i.e., the uncoupled pressure-release cut-on wavenumber solution. Thus, in the presence of fluid–structure coupling, we look for coupled solutions which are a perturbation on this solution.

Fig. 10 shows the schematic of the final results (presented here for clarity). Here, the perturbed PR solution can be seen along with the *in vacuo* structural wavenumber (S=0), the first uncoupled rigid-duct cut-on (R=0) and the first uncoupled pressure-release cut-on (PR=0). Following the steps shown in the small μ case and in [15,16], we use the coupled dispersion relation (Eq. (19)) rewritten in terms of η (different from the frequency-scaling variable used in the case of the coupled structural wavenumber, Eq. (21)) and follow a regular perturbation approach in the unscaled variables. Choosing an asymptotic solution for κ of the form $\kappa = \kappa_0 + \eta a_1 + \nu^2 b_1$ and balancing at orders we obtain closed-form solutions for the leading-order term and the correction terms at $\mathcal{O}(1)$ and $\mathcal{O}(\eta)$,$\mathcal{O}(\nu^2)$, respectively. As expected, the leading-order solution is the same as that obtained from the uncoupled solution for a pressure-release duct as in the second of Eq. (2). The whole solution is given by

$$\kappa = \kappa_0 + \frac{1}{\mu}\frac{\zeta_0^2[-(\kappa_0^2+n^2)^4\beta^2 + \Omega^2(\kappa_0^2+n^2)^2 - \kappa_0^4]}{\Omega^6 c^4 \kappa_0}, \tag{27}$$

where $\zeta_0 = \sqrt{c^2\Omega^2 - \kappa_0^2}$ and κ_0 is found by solving $J_n(\sqrt{c^2\Omega^2 - \kappa_0^2}) = 0$. Again, the correction term corresponding to ν^2 is zero as in the case of the coupled RD cut-on wavenumber for similar reasons, i.e., the effect of Poisson's ratio is a dominantly structural effect and can be expected to appear only at higher orders in the expression for the dominantly acoustic coupled PR wavenumber.

This solution can be seen to become invalid at the uncoupled PR cut-on frequency since κ_0 takes the value zero at this point. Additionally, it is seen that one of the factors of the numerator of the correction term in this expansion corresponds to the term S defined in the coupled dispersion relation (Eq. (20)). Thus, at the uncoupled PR coincidence frequency, S=0 and the correction term is zero, i.e., the uncoupled and coupled PR wavenumbers coincide.

This solution is compared against a numerical solution obtained through a continuation approach as described earlier in this paper. The match is seen to be very good for all the branches (Fig. 11) (Refer Fig. 10 for the schematic). Again, invoking a continuity argument it is seen from the schematic that by progressively increasing the magnitude of the fluid-loading term μ, the coupled rigid-duct cut-on solution obtained earlier in the case for $\mu \ll 1$ transitions continuously to the solution described above for $\mu \gg 1$ and the coupled pressure-release cut-on frequency is now lower than the corresponding uncoupled one. This step brings out the true utility of asymptotic methods in comparison with a numerical solution. Additionally, it is seen that in the presence of fluid–structure coupling, the intersection of the uncoupled wavenumber solutions at the coincidence frequencies is avoided and results in a gap being formed. This phenomenon has been observed earlier in asymptotic [15–17] as well as numerical studies [1–3,28]. This fact is reflected more clearly in the schematic figure (Fig. 13) where the arrows show the direction of movement of the dispersion curves with increasing values of μ. From Fig. 11 it can be seen that the uncoupled and the coupled PR cut-on wavenumbers are very closely spaced. However, for a given Ω, the coupled PR cut-on wavenumber is

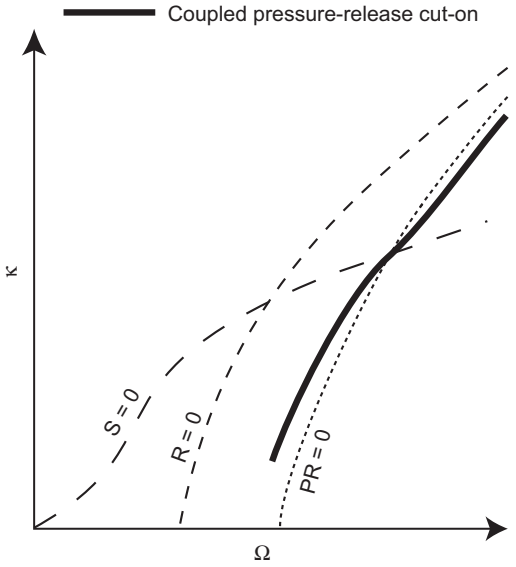

Fig. 10. Schematic of coupled wavenumbers, large μ case.

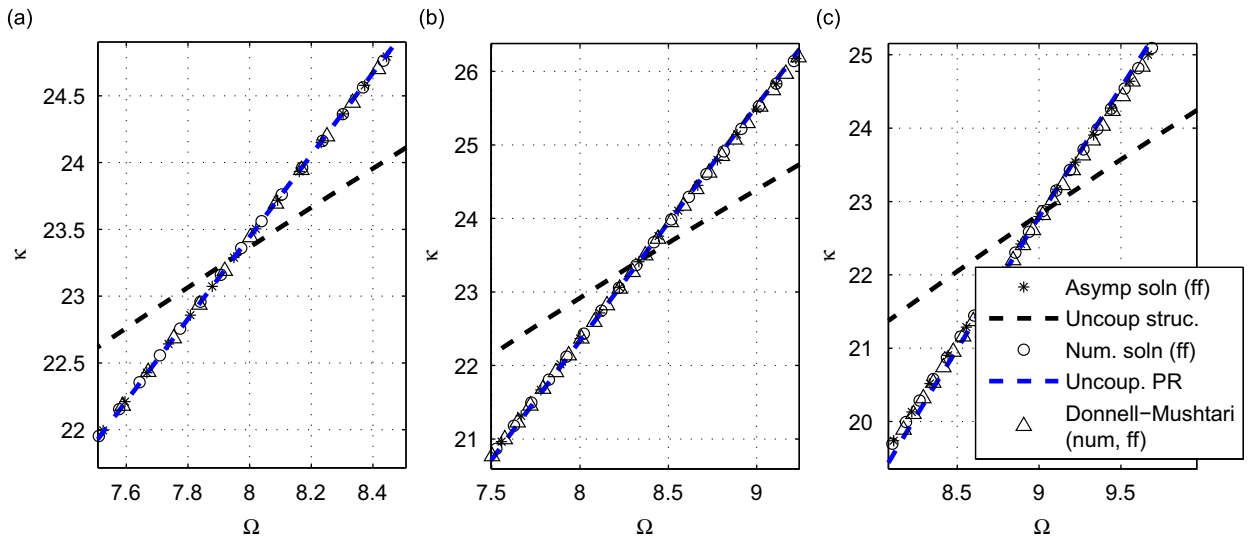

Fig. 11. Coupled pressure-release cut-ons (Eq. (27)—(asymp, ff)), $\beta = 0.0144$, $\nu = 0.3$, $\mu = 10$, c=3; (a) n=2, (b) n=5, (c) n=10. 'ff' stands for 'fluid-filled'.

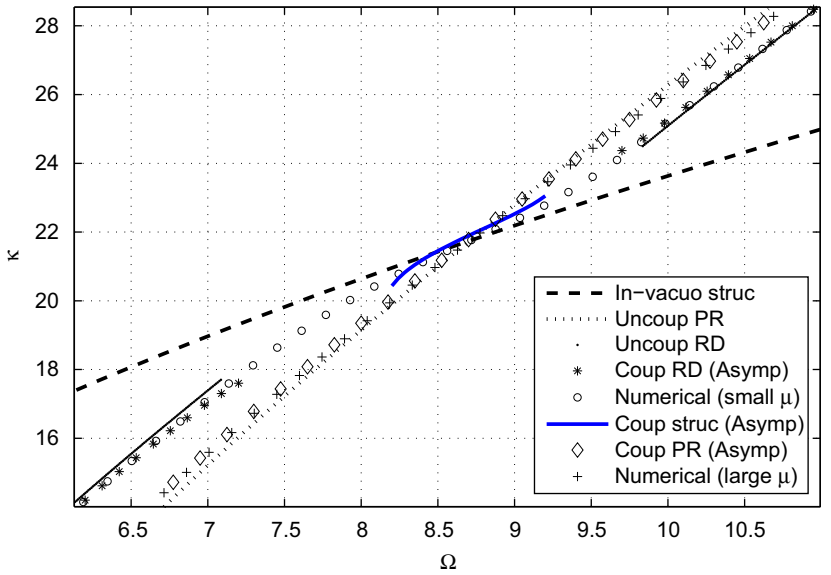

Fig. 12. Integrated plot showing all asymptotic solutions for the coupled case ($\mu = 0.3$, n=10) in the coincidence region along with the corresponding numerical results.

higher in magnitude than the corresponding uncoupled one below the uncoupled PR coincidence frequency and vice versa. The results presented here correspond to a shell with h/a=0.05, i.e., $\beta = 0.0144$.

Fig. 12 shows the asymptotic solutions in the coincidence region for small and large μ (n=10) along with the numerical solution for clarity. The curves for the numerical solution of the DM(ff) theory are not shown here so that the figure does not appear cluttered. However, it has been verified that the numerical solutions for the SST and the DM theory coincide as shown in the other figures.

4. Universal curves

In this section, we study the results obtained thus far in a different fashion, i.e., by the use of constant-frequency loci. These curves are produced by generating a contour plot for the dispersion equation with the circumferential wavenumber on the x-axis and the axial (bending)-wavenumber on the y-axis. The contours are plotted for different frequency values. Universal curves or constant-frequency loci are a particularly insightful way of showing the effect of the curvature in the

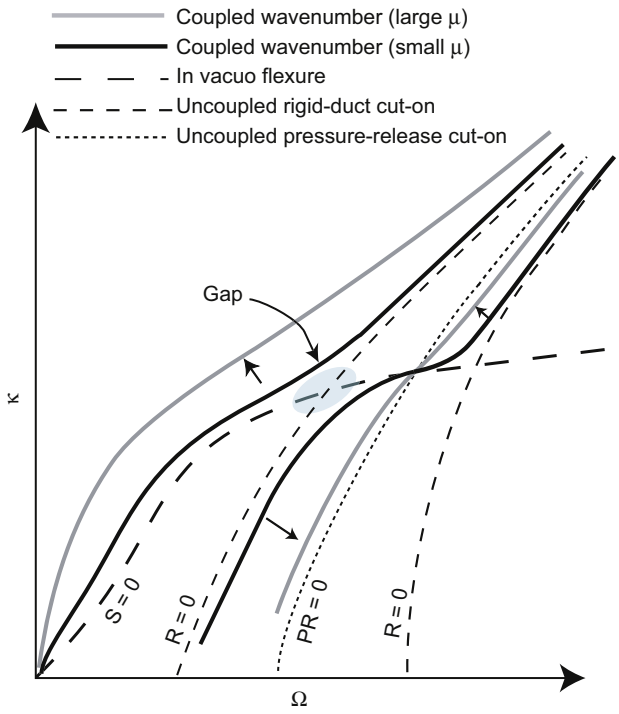

Fig. 13. Schematic of all the obtained results.

shell by separating the membrane and the bending effects [21]. The universal curves for the *in vacuo* plate are circular arcs whereas for shells they get distorted due to the membrane effects. The difference between plates and shells is shown through the constant-frequency loci in [21]. Here, we take a step forward and use this visualization to also compare the coupled dispersion curves of the fluid-filled shell with that of the *in vacuo* shell.

4.1. The in vacuo shell

The universal curves for the *in vacuo* shell are from Eq. (5) with $\nu = 0$ as used by Fahy [21] and are as shown in Fig. 14. As has been shown in the earlier sections, the effect of Poisson's ratio is of $\mathcal{O}(\nu^2)$ and can be neglected without affecting the accuracy of the results. On the x-axis, the circumferential wavenumber is represented by $n\sqrt{\beta}$ and on the y-axis, the axial wavenumber is represented by $\kappa\sqrt{\beta}$. The deviation from the *in vacuo* plate is in the form of veering of the loci towards the origin and is due to the membrane effect. This effect is predominant below the ring frequency. Above the ring frequency, the membrane effects are less pronounced since the wavelength of the circumferential waves is much smaller than the radius of curvature of the shell. As a result, in this region the dynamics of the *in vacuo* shell are similar to that of the *in vacuo* plate and hence the shell curves are almost coincident with the plate curves. This case has been discussed in the literature (see [21, p. 104]) and the curves presented in this sub-section are a reproduction of the results obtained earlier.

4.2. Fluid-filled shell

In this sub-section, we study the effect of fluid–structure coupling on the membrane and bending effects in the shell behaviour through universal constant-frequency loci. In this section as well, we present our results in the manner followed by Fahy [21] in order to highlight the effect of fluid–structure coupling. To this end, we carry over the same simplifications from the previous sub-section, i.e., ν is set to zero as its effect has already been shown to be of $\mathcal{O}(\nu^2)$. Since we are interested in the effect of coupling on the structural wavenumber, we ensure the frequency ranges are chosen so as to only include the coupled structural wavenumber and not the coupled acoustic-duct cut-ons. As has been evidenced by the nature of the asymptotic results obtained and the discussion on MAE, the overall behaviour of the shell is given by patching together the coupled rigid-duct cut-on wavenumber (dominantly acoustic wavenumber) and the coupled structural wavenumber (dominantly structural wavenumber). However, due to the densely clustered nature of the coincidences, the intervals about the coincidence frequencies where the coupled wavenumber is dominantly structural are quite small. As a result, picking points manually in this region (since we are interested in the structural effects) is more prone to error and so we have restricted ourselves to picking points below the first coincidence.

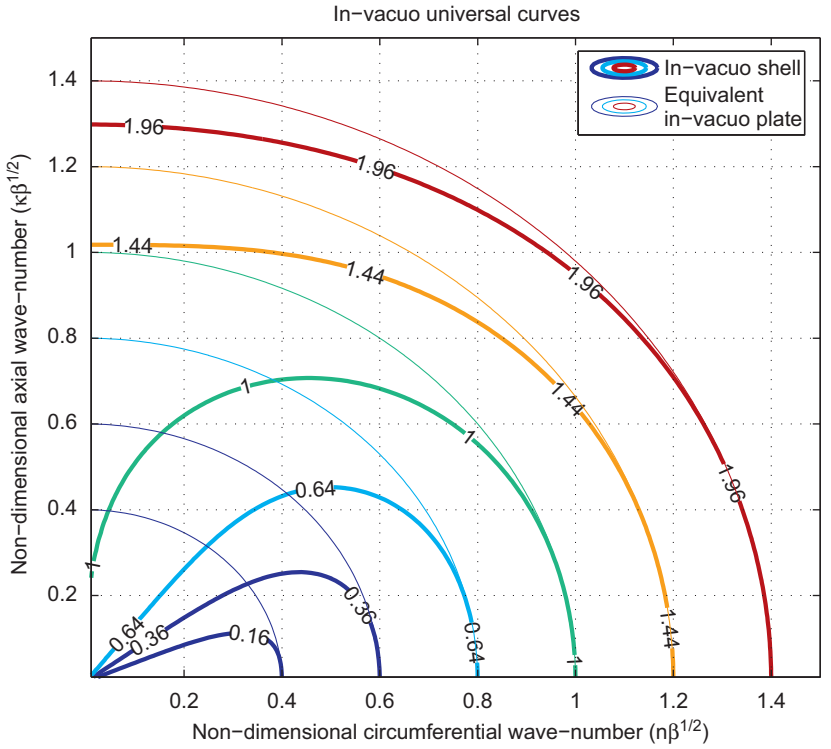

Fig. 14. *In vacuo* constant-frequency loci.

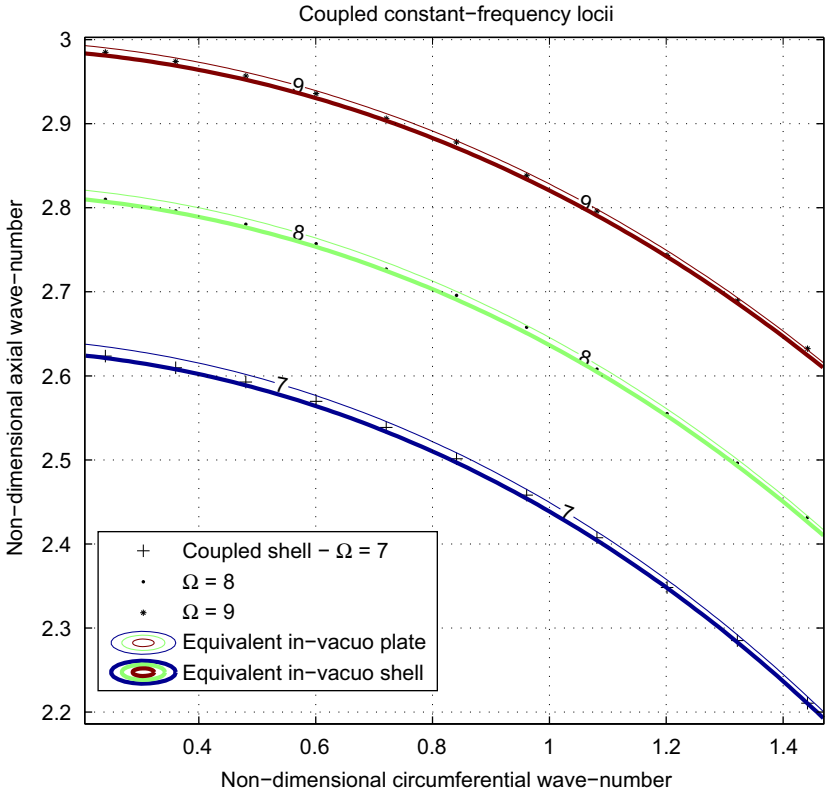

Fig. 15. Coupled constant-frequency loci (lower frequencies), $\mu = 0.3$, c=2.

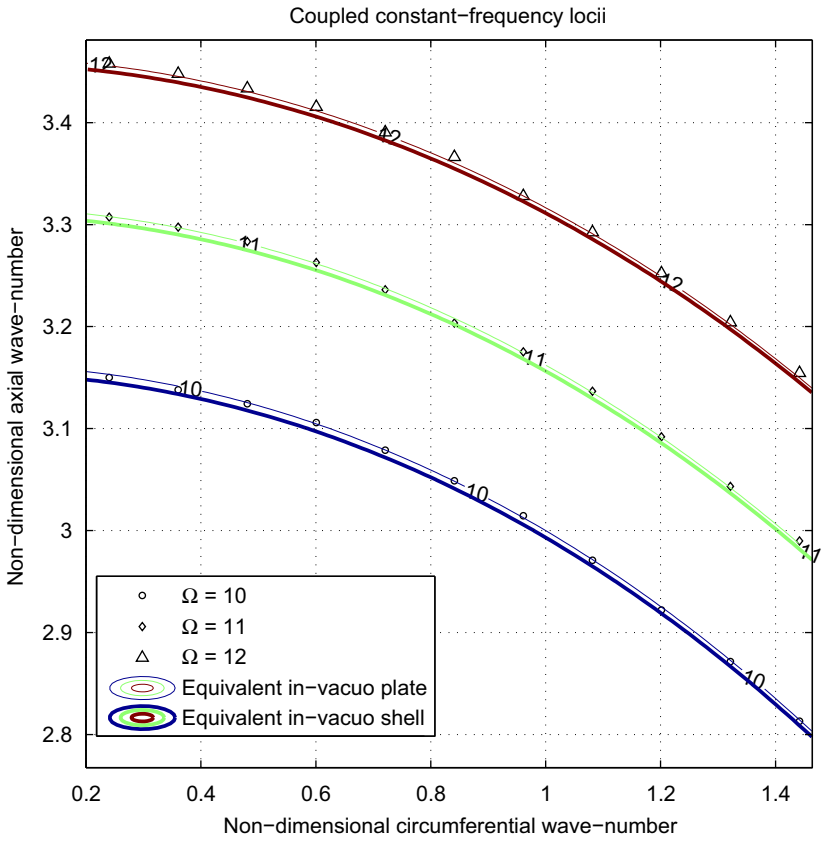

Fig. 16. Coupled constant-frequency loci (higher frequencies), $\mu = 0.3$, c=2.

These results are shown superimposed on a plot containing the constant-frequency loci curves for an equivalent *in vacuo* shell and an equivalent *in vacuo* plate (a plate made of the same material and having the same thickness). As mentioned earlier, since we are only interested in the coupled structural wavenumber, this analysis is restricted to the case where $\mu \ll 1$. From Fig. 15, it is seen that for $\Omega = 7-11$, the constant frequency loci for the coupled shell fall between the corresponding loci for the *in vacuo* shell and the *in vacuo* plate. That is to say, the effect of coupling is to reduce the effect of curvature. This effect can be explained mathematically by considering the governing equation. Rewriting Eq. (20) here for convenience,

$$\underbrace{\frac{\kappa^4}{(n^2+\kappa^2)^2}}_{C} + \frac{\beta^2}{1-\nu^2}(n^2+\kappa^2)^2 - \Omega^2 - \underbrace{\frac{\mu}{(n^2+\kappa^2)^2}\frac{\Omega^6 c^4 J_n(\zeta)}{\zeta J_n'(\zeta)}}_{F} = 0. \tag{28}$$

Here, C is the term which produces the curvature effect while F is the fluid-loading term. Setting both these terms to 0 gives back the equivalent plate equation. For a choice of parameters such that C and F are both positive, it is readily seen that F and C have contradictory effects. Since $(C-F) < C$ for $C > F$, the fluid-filled shell curve is a smaller deviation from the *in vacuo* plate curve as compared to the *in vacuo* shell, i.e., coupling reduces the effect of curvature for these parameter values.

For higher values of Ω (see Fig. 16), the fluid-loaded shell curves cross the *in vacuo* plate curves. The sign of the $(C-F)$ term decides the position of the universal curve for the fluid-loaded shell with reference to the *in vacuo* plate. A schematic of the universal curves is shown in Fig. 17. Crighton in [7] has shown that below coincidence, an infinite 1-D plate loaded by a fluid half-space has its real wavenumber increased due to the fluid-loading. Thus, the universal curves for the fluid-loaded plate are above the *in vacuo* plate. And one can also see that a shell filled with a fluid approaches a fluid-loaded plate in the limit with increasing radius and frequency. Thus, the fluid-filled shell universal curves cross the *in vacuo* plate curves to reach the above limiting case.

5. Conclusions

In this article, we obtain analytical expressions for the coupled wavenumbers in an infinite fluid-filled flexible cylindrical shell modelled using the shallow shell theory (SST). In contrast to the existing literature on the subject where

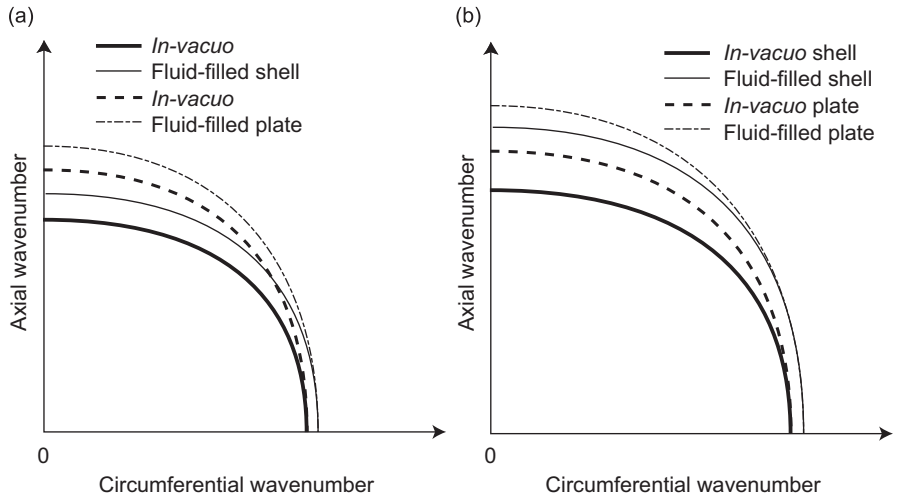

Fig. 17. Schematic of constant-frequency loci for a fluid-filled shell for (a) a low frequency, (b) a high frequency, below coincidence.

typically numerical methods have been used, we use asymptotics to solve the relevant dispersion equation and present the wavenumber expressions. The use of the SST allows us to present the asymptotic formulae in which n, the circumferential mode number appears as a parameter. As a result, a single asymptotic expansion is now valid for all n which is a novel contribution of this work.

Initially, we present asymptotic expressions for the *in vacuo* structural wavenumber in the low and high frequency regions after employing a variable-rescaling approach. These are plotted against numerical solutions to the original *in vacuo* dispersion equation. For the high frequency expansions it is seen that the asymptotic match for a given n is better as the frequency increases.

In the coupled case, we present expressions separately for the small μ and the large μ case. For the small μ case, the solutions are perturbations on the *in vacuo* structural wavenumber and the uncoupled acoustic rigid-duct cut-on. The regular expansion for the coupled structural wavenumber becomes invalid (blows up) at the rigid-duct coincidences but remains finite around the pressure release coincidences. Exactly at the pressure-release coincidence, the correction term in this expansion is zero so that the *in vacuo* structural wavenumber and the coupled structural wavenumber are equal here. The regular expansion for the coupled rigid duct cut-on becomes invalid at the rigid duct coincidences, where an alternative expansion can be found. Thus, a coupled rigid duct cut-on transitions into the coupled structural wavenumber passing through the pressure release coincidence and back to the next coupled rigid duct cut-on. This way the full coupled branch remains continuous despite individual expansions becoming invalid. An outcome of this patching of solutions is that the coupled wavenumbers do not intersect anymore, a gap is created where earlier their uncoupled counterparts intersected. Comparisons of the above expansions with numerical solutions show a good match, specially at higher frequencies.

For the large μ case, we again present an asymptotic solution to the coupled dispersion equation which is a perturbation on the uncoupled pressure-release cut-on. The solution thus obtained is seen to be valid for all frequencies (except at the pressure release cut-on frequency). This solution is compared with the numerical solution of the dispersion relation and the match is seen to be good over the entire frequency range.

Further, all the asymptotic results obtained using the SST in this article have also been compared with numerical solutions of the dispersion relation obtained by using a more general theory, namely, the Donnell–Mushtari theory which is a commonly used thin shell theory. The match with these solutions is also very good, validating the use of the SST to model the shell behaviour and the use of asymptotic methods to solve for the wavenumbers.

It is found that in comparison to the uncoupled case, the coupled rigid duct cut-on frequency is raised, whereas the coupled pressure release cut-on frequency is lowered. The transition of solutions from small μ to large μ has also been shown, again by invoking a continuity argument.

In each of the above cases, the effect of Poisson's ratio ν has been included in our calculations; ν^2 is also used as an expansion variable while finding the asymptotic solution for the wavenumber. Thus, the effect of ν is of $\mathcal{O}(\nu^2)$ or higher. In the uncoupled and coupled structural wavenumbers, the effect of Poisson's ratio is seen at $\mathcal{O}(\nu^2)$, implying that the effects of Poisson's ratio and the fluid-coupling are of comparable orders. However, in the case of the coupled acoustic wavenumbers, the coefficient of ν^2 was seen to be uniformly zero. Thus, the effect of the fluid–structure interaction is a more dominant effect and the effect of ν will be seen only at higher orders.

Finally, we present the solutions in the form of universal constant-frequency loci. Here, we compare the universal curves for the *in vacuo* and the coupled small μ cases. The constant frequency loci for the coupled shell fall between the corresponding loci for the *in vacuo* shell and the *in vacuo* plate. The effect of coupling is thus to reduce the effect of

curvature. However, for higher values of Ω (see Fig. 16), the fluid-loaded shell curves cross the *in vacuo* plate curves. This happens because the fluid-filled shell wavenumbers tend to approach those of a plate loaded by a half-space of fluid.

References

[1] C.R. Fuller, The input mobility of an infinite circular cylindrical elastic shell filled with fluid, *Journal of Sound and Vibration* 87 (1983) 409–427.
[2] C.R. Fuller, F.J. Fahy, Characteristics of wave propagation and energy distributions in cylindrical elastic shells filled with fluid, *Journal of Sound and Vibration* 81 (1982) 501–518.
[3] G. Pavic, Vibrational energy flow in elastic circular cylindrical shells, *Journal of Sound and Vibration* 142 (1990) 293–310.
[4] J.M. Muggleton, M.J. Brennan, P.W. Linford, Axisymmetric wave propagation in fluid-filled pipes: wavenumber measurements in in vacuo and buried pipes, *Journal of Sound and Vibration* 270 (2004) 171–190.
[5] M. Maess, N. Wagner, L. Gaul, Dispersion curves of fluid filled elastic pipes by standard fe models and eigenpath analysis, *Journal of Sound and Vibration* 296 (2006) 264–276.
[6] M.B. Xu, X.M. Zhang, Vibration power flow in a fluid-filled cylindrical shell, *Journal of Sound and Vibration* 218 (1998) 587–598.
[7] D.G. Crighton, The 1988 Rayleigh medal lecture: fluid-loading—the interaction between sound and vibration, *Journal of Sound and Vibration* 133 (1989) 1–27.
[8] D. Innes, D.G. Crighton, Power radiated by an infinite plate subject to fluid-loading and line-drive, *Journal of Sound and Vibration* 123 (1988) 437–450.
[9] D.G. Crighton, D. Innes, Low-frequency acoustic radiation and vibration response of locally excited fluid-loaded structures, *Journal of Sound and Vibration* 91 (1983) 293–314.
[10] D.G. Crighton, The free and forced waves on a fluid-loaded elastic plate, *Journal of Sound and Vibration* 63 (1979) 225–235.
[11] S.V. Sorokin, S.G. Kadyrov, Modelling of nonlinear oscillations of elastic structures in heavy fluid loading conditions, *Journal of Sound and Vibration* 222 (1999) 425–451.
[12] S.V. Sorokin, Nonlinear oscillations of a baffled elastic plate in heavy fluid loading conditions, *Journal of Sound and Vibration* 232 (2000) 619–643.
[13] S.V. Sorokin, C.J. Chapman, The forced vibration of an elastic plate under significant fluid loading, *Journal of Sound and Vibration* 281 (2005) 719–741.
[14] S.V. Sorokin, C.J. Chapman, Asymptotic analysis of nonlinear vibration of an elastic plate under heavy fluid loading, *Journal of Sound and Vibration* 284 (2005) 1131–1144.
[15] A. Sarkar, V.R. Sonti, Asymptotic analysis for the coupled wavenumbers in an infinite fluid-filled flexible cylindrical shell: the axisymmetric mode, *Computer modeling in Engineering and Sciences* 21 (3) (2007) 193–207.
[16] A. Sarkar, V.R. Sonti, Asymptotic analysis for the coupled wavenumbers in an infinite fluid-filled flexible cylindrical shell: the beam mode, *Journal of Sound and Vibration* 319 (2009) 646–667.
[17] A. Sarkar, V.R. Sonti, Wave equations and solutions of *in vacuo* and fluid-filled elliptic cylindrical shell, *International Journal of Acoustics and Vibration* 14 (1) (2009) 35–45.
[18] E.J. Hinch, *Perturbation Methods*, Cambridge University Press, 1991.
[19] W. Soedel, *Vibration of Plates and Shells*, Marcel-Dekker International, 2000.
[20] M. Heckl, Vibrations of point-driven cylindrical shells, *Journal of the Acoustical Society of America* 14 (10) (1962) 1553–1557.
[21] F.J. Fahy, *Sound and Structural Vibration: Radiation, Transmission and Response*, Academic Press, 1989.
[22] A. Sarkar, V.R. Sonti, Simplified dispersion curves for circular cylindrical shells using shallow shell theory, *Journal of Sound and Vibration* 322 (2009) 1–7.
[23] L.E. Kinsler, A.R. Frey, A.B. Coppens, J.V. Sanders, *Fundamentals of Acoustics*, John Wiley & Sons, Inc., 2000.
[24] C.S. Jog, *Foundations and Applications of Mechanics—Volume I, Continuum Mechanics*, Narosa Publishing House, 2007.
[25] A.W. Leissa, Vibration of shells, Technical Report NASA SP-288, 1973.
[26] A.H. Nayfeh, *Perturbation Methods*, John Wiley & Sons, 1973.
[27] A. Sarkar, Asymptotic Analysis of Dispersion Characteristics of Structural Acoustic Waveguides, Ph.D. Thesis, I.I.Sc., Bangalore, 2009.
[28] A. Cabelli, The propagation of sound in a square duct with a non-rigid side wall, *Journal of Sound and Vibration* 103 (1985) 379–394.